An Examination of Propagation Effects in Rainfall on Radar Measurements at Microwave Frequencies

V. N. BRINGI

Colorado State University, Fort Collins, Colorado

V. CHANDRASEKAR

University of Alabama in Huntsville, Huntsville, Alabama

N. BALAKRISHNAN* AND D. S. ZRNIĆ

NOAA/ERL, National Severe Storms Laboratory, Norman, Oklahoma

(Manuscript received 10 January 1990, in final form 19 June 1990)

ABSTRACT

Propagation effects in rainfall are examined at three microwave frequencies corresponding to S (3.0 GHz), C (5.5 GHz), and X (10.0 GHz) bands. Attenuation at horizontal polarization, as well as differential attenuation and differential propagation phase between horizontal (H) and vertical (V) polarizations are considered. It is shown that at the three frequencies both attenuation and differential attenuation are nearly linearly related to differential propagation phase (ϕ_{DP}). This is shown through simulation using (a) gamma raindrop size distributions (RSD) with three parameters (N_0, D_0, m) that are varied over a very wide range representing a variety of rainfall types, and (b) measured raindrop size distributions at a single location using a disdrometer. Measurements of X-band specific attenuation and S-band specific differential phase in convective rainshafts using the National Center for Atmospheric Research CP-2 radar are presented in order to experimentally demonstrate the linear relationship between attenuation and differential propagation phase. Correction procedures for reflectivity and differential reflectivity (Z_{DR}) are developed assuming that differential propagation phase is measured using a radar that alternately transmits H and V polarized waves with copolar reception through the same receiver and processor system. The correction procedures are not dependent on the actual rainrate profile between the radar and the range location of interest. The accuracy of the procedure depends on, (a) RSD fluctuations, (b) variability in the estimate of differential propagation phase due to measurement fluctuations, and (c) nonzero values of the backscatter differential phase (δ) between H and V polarizations. Simulations are used to gauge the accuracy of correction procedures at S- and C-bands assuming δ is negligible. The correction accuracy for attentuation at S-band is estimated to be ~0.05 dB while at C-band it is estimated to be within 1 dB if $\phi_{DP} \leqslant 60°$. Simulations further indicate that C-band differential attenuations effects can be corrected to within ~35% of the mean value.

1. Introduction

Radars that operate at higher frequencies such as C- or X-band offer the advantage of lower cost resulting from smaller antenna size compared to S-band radars having the same spatial resolution. Also, higher frequencies are preferred, since the power returned by atmospheric scatterers is inversely proportional to the fourth power of the wavelength (Doviak and Zrnić

1984). However, the resulting gain in sensitivity and spatial resolution is vastly offset by attenuating precipitation. Quantitative interpretation of echo powers at higher frequencies requires correction for this attenuation.

Hitschfeld and Bordan (1954) showed that an indirect estimate of the specific attenuation A (attenuation in dB over 1 km distance), due to the scatterers can be obtained using empirical relationships such as Z–R (between the reflectivity factor Z and rain rate R) and A–R (between attenuation constant, A and R). In their scheme, the correction for the attenuation of the power received from the nth range location is done using the reflectivity measurements made at all the preceding ($n - 1$) range locations. The attenuation correction is first invoked for the range location nearest to the radar and then at successive range locations. Hitschfeld and Bordan also demonstrated that at 3 cm

---

and to some extent at 5.6 cm wavelength, a small error in the radar calibration constant causes a large error in the measured rain rate. Further, this error, which varies with range is liable to be more serious than that caused if attenuation is entirely neglected, thus rendering attenuation correction entirely useless (Hitschfeld and Bordan 1954).

With the advent of polarization agile radars, a better estimate of R, and hence A, is possible than with Z alone. Aydin et al. (1986) derived an empirical relationship to estimate A_H (specific attenuation at horizontal polarization) from Z_H (reflectivity at H-polarization) and Z_{DR} (differential reflectivity) and proposed a correction scheme for C-band data. They noted that the procedure was very sensitive to biases (which include calibration errors) in the measurements of Z_H and Z_{DR}. All the techniques for attenuation correction, to date, are essentially similar to those proposed by Hitschfeld and Bordan (1954) in that (a) they use reflectivity estimates Z_H or Z_V, or both to obtain an estimate of attenuation by the scatterers in a resolution volume, (the reflectivity estimates themselves being affected by attenuation) and (b) they employ the correction at the nth range location based on the corrected reflectivity measurements at all the preceding locations. In other words, the correction is applied at successive range locations, starting from the one that is nearest to the radar, (see also Hildebrand 1978).

Dual wavelength radars use both 10-cm and 3-cm wavelengths. This has the advantage that reflectivity estimates unaffected by attenuation are available at all range locations from the 10-cm radar. However, the attenuation correction to the 3-cm reflectivity, and hence to the dual wavelength ratio (DWR), is done by apportioning the total attenuation along the radial using an empirical A-Z_H(S) relation; Z_H(S) is the reflectivity factor for horizontal polarization at S-band. The attenuation correction at any range location is thus dependent on the reflectivity factor at all the other range locations (Tuttle and Rinehart 1983).

With the recent advent of a number of polarimetric radars at C- and X-bands it is important to consider not only absolute attenuation in rainfall but also differential attenuation (α_{DP}) and differential propagation phase (ϕ_{DP}) between the two principal polarization states. These are the horizontal (H) and vertical (V) states for an equioriented, oblate raindrop model whose symmetry axis is closely oriented along the V-direction; McCormick (1975), Oguchi (1983). It has long been known that even at S-band the differential propagation phase in rainfall can cause severe depolarization of a transmitted circularly polarized wave, Humphries (1974). McGuiness et al. (1987) attempted to correct the circular depolarization ratio (CDR) using an iterative range location-by-range location procedure that they found to be numerically unstable. Bebbington et al. (1987) developed a new procedure based on the coherency matrix transformation which avoids the use

of an iterative procedure. Subsequently, Holt (1988) showed that Z_{DR} could be corrected for the very small differential attenuation at S-band by assuming a linear relationship between α_{DP} and ϕ_{DP}. The approach adopted here is similar to Holt's (1988) in that both the absolute attenuation (α_H or α_V) as well as the differential attenuation (α_{DP}) are linearly related to ϕ_{DP} in rainfall. Whereas Holt (1988) derives Z_{DR} and ϕ_{DP} using circular polarization observables obtained with dual-channel reception, it is assumed here that Z_{DR} and ϕ_{DP} are obtained using "fast" polarization switching between H and V states with copolar reception through the same receiver and processor, Seliga and Bringi (1976, 1978) and Sachidananda and Zrnić (1989). The algorithm used to estimate ϕ_{DP} assumes that the differential phase shift due to backscatter is negligible, Mueller (1984) and Jameson and Mueller (1985). Although this is true for raindrops at S-band, it is not so at C- and X-bands. This factor places an upper limit on the accuracy of the correction procedure based on ϕ_{DP} in inhomogeneous regions of rainfall.

McCormick and Hendry (1975) have shown that the range profile of the complex observable W/W_2 can be used to directly estimate α_{DP} and ϕ_{DP} in a variety of precipitation media. The quantity W is the complex cross-correlation between the two simultaneously received, circularly polarized waves and W_2 is the conventional reflectivity proportional to the cross-polar received power. Observations at Ku, X-, and S-bands have been presented by McCormick and Hendry (1975), Hendry and Antar (1984), and Hendry et al. (1976). These studies were aimed at particle identification and for modeling of propagation paths and were thus not used to correct the backscatter observables such as CDR or reflectivity (W_2). It is only recently that S-band circular polarization data have been used to derive linearly polarized observables; e.g., Z_{DR}, unaffected by ϕ_{DP} effects, Bebbington et al. (1987), Holt (1988) and Jameson and Dave (1988). It is conventional to assume that absolute attenuation at S-band is negligible. However, when ϕ_{DP} is large and when accurate reflectivity estimates are needed (± 1 dB) it is not possible to neglect the attenuation. For example, when $\phi_{DP} = 90°$ as may be due to a uniform rainrate of 73 mm h^{-1} over a 22.5 km path, the attenuation at S-band is estimated to be ~ 2 dB. Thus, it would be important to correct for this attenuation whenever the measured reflectivity is used in rainfall rate algorithms; e. g., the NEXRAD hydrology algorithms, especially under rainfall conditions typically found in squall lines and mesoscale convective complexes (MCC). From this perspective, a case could be made for the implementation of ϕ_{DP} measurements on NEXRAD.

A substantial body of literature exists on the measurement and modeling of attenuation and depolarization effects along terrestrial and satellite–earth paths at microwave and millimeter wave frequencies; see, for example, Oguchi (1983) and the comprehensive

reference list therein. S-band differential reflectivity radar data have been used to model rain attenuation along satellite–earth paths at higher frequencies, to calculate attenuation ratios (frequency scaling), and to estimate site diversity gain, Leitao and Watson (1984), Holt et al. (1984), Goddard and Cherry (1984) and Marshall et al. (1984). The basic method is to combine reflectivity and Z_{DR} to estimate the parameters N_0 and D_0 of an exponential raindrop size distribution (RSD), and subsequently to calculate the path attenuation. In this context it is possible to identify backscatter observables such as Z_H and Z_{DR} that measure the variability of the rain medium as a function of range as opposed to forward scatter observables such as α_H and ϕ_{DP} that increase cumulatively with increasing penetration into the rain medium. Prediction and correction procedures based on backscatter observables are more sensitive to RSD fluctuations as compared to those based on forward scatter observables; Atlas et al. (1984) and Sachidananda and Zrnić (1987). The physical differences between the two approaches is rooted in the fact that an incoherent process is responsible for the backscatter observables, whereas the forward scatter process is coherent; Ishimaru (1977). Thus, under the first-order multiple scattering approximation (which is generally valid for rainfall at radar frequencies) the rain medium in which the coherent wave propagates can be modeled in an average or bulk sense by complex, propagation constants k_H and k_V; Twersky (1978), Bringi et al. (1983). Thus, prediction and correction procedures based on ϕ_{DP} are likely to be more stable than those based on iterative range location-by-range location methods.

This paper is organized as follows: section 2 describes the simulation of gamma RSDs with parameter fluctuations as derived by Ulbrich (1983) for natural rainfall. Scatterplots of specific attenuation (A_H, dB km^{-1}) and differential attenuation (A_{DP}, dB km^{-1}) versus specific differential phase (K_{DP}, ° km^{-1}) are presented at S-, C- and X-band frequencies. In section 3, disdrometer measured RSDs are used to simulate attenuation and differential attenuation versus ϕ_{DP} at the three radar frequencies. In section 4 radar measurements of X-band specific attenuation versus S-band K_{DP} are presented in convective rainshafts using the NCAR CP-2 radar. These data are compared with the simulations. In section 5 correction procedures for reflectivity and differential reflectivity at S- and C-bands are simulated based on ϕ_{DP}. These simulations include both gamma RSD fluctuations as well as random measurement errors. A summary of results and conclusions end the paper.

2. Calculations based on gamma distributions

Ulbrich (1983) has shown that the gamma model can adequately describe many of the natural variations

in the RSD. This model has three parameters and is given by

$$N(D) = N_0 D^n \exp[-(3.67 + n)D/D_0] \quad (1)$$

where D is the volume equivalent spherical diameter and D_0 is termed the median volume diameter of the distribution.

The specific differential phase (K_{DP}) is defined as

$$K_{DP} = \frac{180\lambda}{\pi} \int \mathrm{Re}[f_H(D) - f_V(D)]N(D)dD,$$

where λ is the wavelength, and f_H and f_V are the forward scattering amplitudes for horizontally and vertically polarized waves. The one-way differential propagation phase (ϕ_{DP1}) between two range locations r_1, r_2 is defined as

$$\phi_{DP1} = \int_{r_1}^{r_2} K_{DP}(r)dr. \quad (3)$$

The two-way differential propagation phase ϕ_{DP} equals $2\phi_{DP1}$.

The specific attenuation at H or V polarizations is defined as

$$A_{H,V} = 0.4343 \int Q_{H,V}(D)N(D)dD, \quad \mathrm{dB\ km^{-1}}$$
$$(4)$$

where $Q_{H,V}(D)$ are the extinction cross sections for H and V polarized waves. The specific differential attenuation is $A_{DP} = A_H - A_V$, dB km^{-1}, and the one-way differential attenuation (α_{DP1}) is defined as

$$\alpha_{DP1} = \int_{r_1}^{r_2} A_{DP}(r)dr. \quad (5)$$

The two-way differential attenuation α_{DP} ($=\alpha_H - \alpha_V$) is defined as being equal to $2\alpha_{DP1}$.

The reflectivities $Z_{H,V}$ at horizontal (H) and vertical (V) polarizations, respectively, are defined as

$$Z_{H,V} = \frac{\lambda^4}{\pi^5 |K|^2} \int \sigma_{H,V}(D)N(D)dD, \quad \mathrm{mm^6\ m^{-3}}$$
$$(6)$$

where $\sigma_{H,V}(D)$ are the radar cross sections at H and V polarizations, λ is the wavelength, $K = (\epsilon_r - 1)/(\epsilon_r + 2)$ and ϵ_r is the refractive index of water. Differential reflectivity (Z_{DR}) is defined as

$$Z_{DR} = 10 \log(Z_H/Z_V), \quad \mathrm{dB}. \quad (7)$$

If $S_H(D)$ and $S_V(D)$ are the principal plane elements of the backscatter matrix, (i.e., when the raindrop minor axis is along the V-polarization direction) then the cross correlation coefficient ρ_{HV} can be defined as
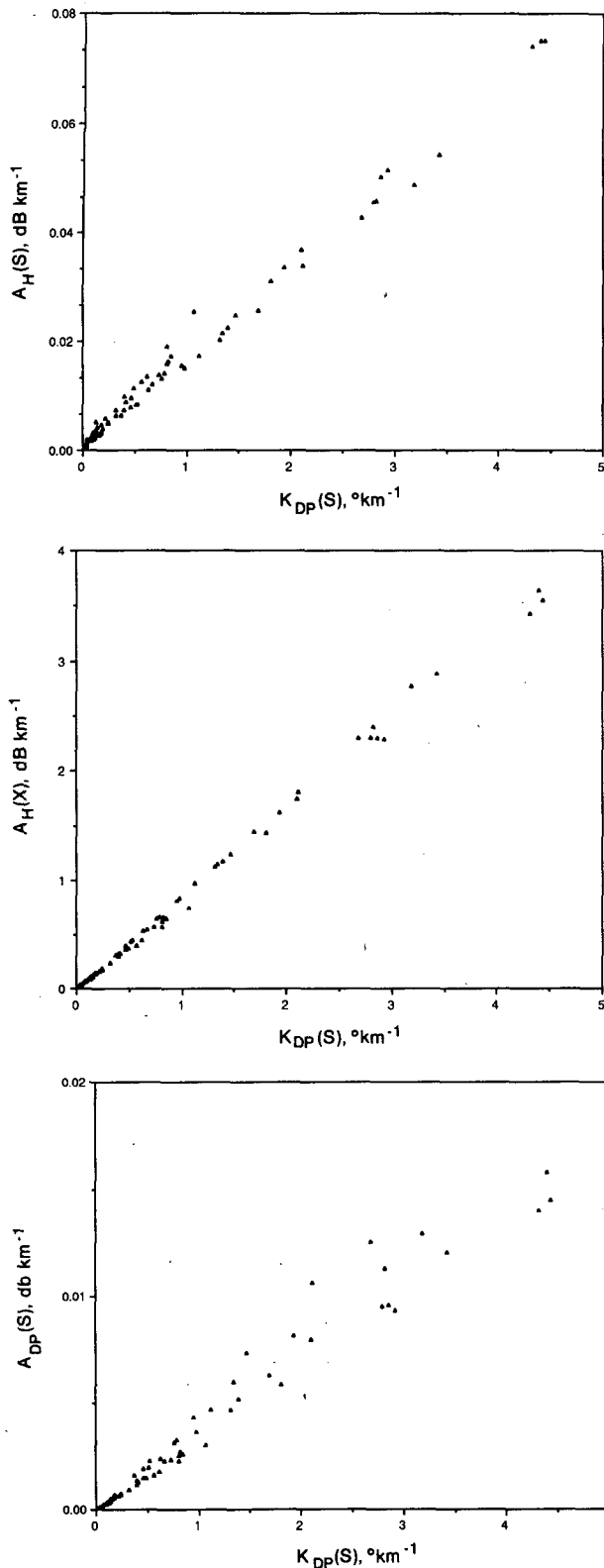
$$\rho_{HV} = \frac{\int S_H(D)S_V^*(D)N(D)dD}{[\int |S_H|^2 N(D)dD]^{1/2} [\int |S_V|^2 N(D)dD]^{1/2}}.$$

(8)

Further, $\rho_{HV} = |\rho_{HV}| \exp(j\delta)$ where δ is defined as the backscatter differential phase shift for a H–V basis. McCormick and Hendry (1975) have defined a related parameter termed the scattering differential phase shift for circular polarization basis. Nonzero values of δ imply non-Rayleigh scattering effects; McCormick et al. (1979). Jameson (1985) has shown that $\delta \approx 0^c$ for raindrops at S-band.

The quantities A_H, A_{DP}, K_{DP}, Z_{DR} and δ are computed for gamma RSDs. The gamma parameters (N_0, D_0, n) are varied as follows: $0 < D_0 \leq 2.5$ mm, $-1 < n \leq 4$, $10^{4.2} \exp(2.8n) \leq N_0 \leq 10^{5.5} \exp(3.57n)$, m^{-3} mm$^{(-1-n)}$; Ulbrich (1983). For each triplet of values (N_0, D_0, n) the propagation and backscatter variables are computed using (2)–(8). Raindrops are modeled by oblate spheroids with axis ratios as given by Green (1975). The maximum drop diameter is 8 mm. The three frequencies considered are 3.0 (S-band), 5.5 (C-band), and 10.0 GHz (X-band). The refractive index of water at a temperature of 15°C and at the three frequencies was taken from Ray (1972). Figures 1a–c show simulations of (a) $A_H(S)$, (b) $A_H(X)$, and (c) $A_{DP}(S)$ versus $K_{DP}(S)$. The scatter reflects the variations imposed on the RSD parameters. Both $A_H(S)$ and $A_H(X)$ are linearly related to $K_{DP}(S)$ with very little scatter whereas $A_{DP}(S)$ shows somewhat larger scatter. The fact that the simulation shows considerable scatter around the mean linear relationship between K_{DP} and A_{DP}, is in line with the observations of Jameson (1989). Jameson (1989) has shown that K_{DP} at 2.2 cm wavelength is approximately proportional to the integral over the RSD of $(1 - r)D^3$, while A_{DP} is proportional to the integral of $(1 - r)D^4$, r being the axis ratio of the rain drop. This implies that the linear relationship between K_{DP} and A_{DP} is never exact. Later we will show, for comparison, CP-2 radar measurements of $A_H(X)$ versus $K_{DP}(S)$. The linear relationship between $A_H(S)$ versus $K_{DP}(S)$ as seen in Fig. 1a can be used to estimate the attenuation at H-polarization experienced by S-band radar (such as NEXRAD) as function of ϕ_{DP}. This result is shown in Fig. 2.

The attenuation is less than 1 dB if $\phi_{DP} \leq 60°$, and about 2 dB for $\phi_{DP} = 120°$. Thus, if reflectivity estimates with bias less than 1 dB are desired then a correction scheme could be implemented based on the measured ϕ_{DP}. As long as A_H and K_{DP} are linearly re-

FIG. 1. (a) Simulations of specific attenuation at H-polarization versus specific differential phase. Each data point refers to one particular value of the triplet of gamma RSD parameters (N_0, D_0, n). The scatter reflects the effects of a large variety of raindrop size dis-

tributions and hence of rainfall types. Calculations are at S-band. (b) As in Fig. 1a except the ordinate scale is X-band specific attenuation at H-polarization. Note $A_H = 0.8K_{DP}$. The correlation coefficient is 0.998. (c) As in Fig. 1a except the ordinate scale is the S-band specific differential attenuation between H and V polarizations, $A_{DP} = A_H - A_V$.
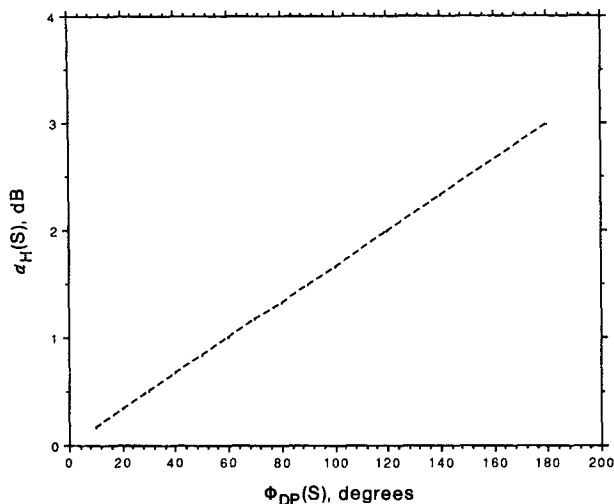
FIG. 2. Two-way attenuation at H-polarization, α_H, versus the two-way differential propagation phase between H and V-polarizations, ϕ_{DP}. Calculations are at S-band.

lated, this correction scheme would be independent of the actual rainrate profile along the propagation path. Figure 1c shows that a correction scheme for $Z_{DR}(S)$ would be needed if $\phi_{DP} \gtrsim 55°$. This follows from the linear relationship $A_{DP}(S) = \beta K_{DP}(S)$ where β is the slope; thus, $\alpha_{DP}(S) = \beta\phi_{DP}(S)$. From Fig. 1c the slope $\beta = 3.67 \times 10^{-3}$ dB per degree, and for $\alpha_{DP} = 0.2$ dB we get $\phi_{DP} = 55°$. Table 1 presents the mean linear relationships obtained from Figs. 1, 3, and 5. The mean linear relationships are given in terms of the slope β and correlation coefficient ρ in Table 1. A Z_{DR} correction scheme based on ϕ_{DP} appears feasible and in fact was suggested by Holt (1988). We reiterate that ϕ_{DP} and Z_{DR} are assumed here to be measured using fast switching between H and V polarization with copolar reception.

Figures 3a,b show scatterplots of (a) $A_H(C)$ versus $K_{DP}(C)$, and (b) $A_{DP}(C)$ versus $K_{DP}(C)$. In both cases the scatter has increased compared to the S-band results. However, a mean linear relationship (see Table 1) between $A_H(C)$ and $K_{DP}(C)$ exists with slope $\beta = 0.054$; thus, $\alpha_H(C) = 0.054\phi_{DP}(C)$. If $\phi_{DP} \leq 20°$, then the two-way C-band attenuation at H-polarization, $\alpha_H(C)$, is less than 1 dB. From Fig. 3b a mean

TABLE 1. Mean linear relationships obtained using gamma raindrop size distributions. β is in dB per degree and ρ is the correlation coefficient.

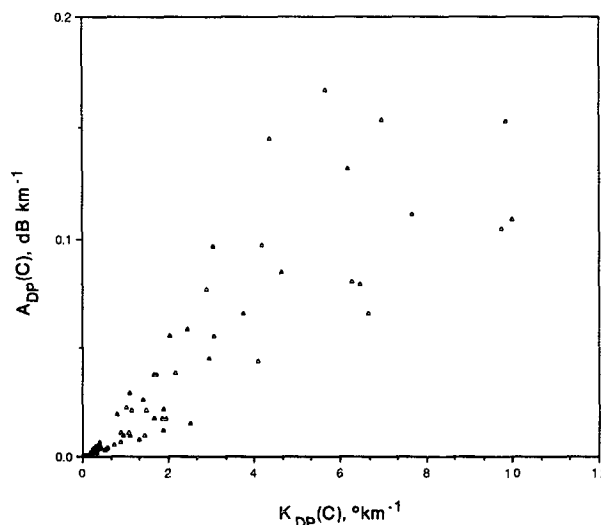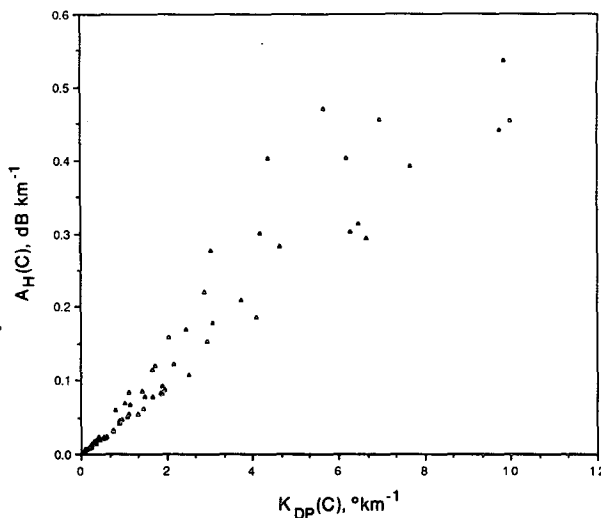| Relation	Frequency band					
	S (3.0 GHz)		C (5.5 GHz)		X (10.0 GHz)	
	β	ρ	β	ρ	β	ρ
$A_H = \beta K_{DP}$	0.016	0.99	0.054	0.94	0.25	0.99
$A_{DP} = \beta K_{DP}$	0.00367	0.98	0.0157	0.82	0.05	0.97

FIG. 3. (a) As in Fig. 1a except simulations are at C-band. (b) As in Fig. 1c except simulations are at C-band.

linear relationship of the form $\alpha_{DP}(C) = 0.0157\phi_{DP}(C)$ can be derived. Considerable fluctuation about this mean relationship due to variations in the RSD parameters is noted. Furthermore, the RSD parameter variations imposed here encompass a wide range of rainfall types, but within a given rainfall type the variations may be lower; Ulbrich (1983). We raise this point again in section 3. From Fig. 3b, a ϕ_{DP} of 15° gives mean $\alpha_{DP} = 0.24$ dB; thus, the extreme bounds due to RSD variability are 0.42 and 0.14 dB. From a practical viewpoint correction for $Z_H(C)$ and $Z_{DR}(C)$ does not appear to be necessary if $\phi_{DP}(C) \leq 20°$. At S-band the corresponding result is $\phi_{DP}(S) \leq 60°$.

In principle, correction for $Z_H(C)$ and $Z_{DR}(C)$ can be attempted if $\phi_{DP}(C)$ can be measured accurately. However, Fig. 4 shows that the backscatter differential phase shift, $\delta(C)$, may not be negligible when $Z_{DR} \gtrsim 2.5$ dB. As shown by Mueller (1984), in the presence

of propagation effects $\arg(\hat{\rho}_{HV}) = \phi_{DP} + \delta$ where $\hat{\rho}_{HV}$ is obtained from radar data. The correction accuracy will depend on how accurately $\phi_{DP}(C)$ can be estimated given the measured range profile of $\arg(\hat{\rho}_{HV})$. This problem is conceptually similar to the estimation of attenuation and hail signal given the range profile of dual-frequency reflectivity ratio (DFR), which is the difference between the range normalized received powers at S- and X-bands; Tuttle and Rinehart (1983), Eccles and Mueller (1973), Eccles (1979) and Jameson and Srivastava (1978). The DFR range profile is used to estimate X-band attenuation in rainfall assuming that Rayleigh scattering holds at both frequencies. The profile of $\arg(\hat{\rho}_{HV})$ is similar in nature to the DFR profile discussed in section 4, (see Fig. 9). It is well known that nonzero δ implies non-Rayleigh scattering; McCormick et al. (1979). Thus, in the presence of large raindrops or oblate, melting hail the range profile of $\arg(\hat{\rho}_{HV})$ will be monotonically increasing with "bumps" superimposed near locations of nonzero δ; see Meischner et al. (1989). From Fig. 4 we see that $\delta(C)$ can be estimated if $Z_{DR}(C)$ is known. However, the accuracy with which $\delta(C)$ can be estimated depends on the accuracy of the $Z_{DR}(C)$ correction procedure. When $\phi_{DP}(C) \gtrsim 90°$, the relative contribution of $\delta(C)$ to $\arg(\hat{\rho}_{HV})$ decreases and thus its effects on the estimators of α_H or α_{DP} are less significant. However, the estimate of $K_{DP}(C)$ over a small range interval will be affected by $\delta(C)$ over that range irrespective of the ϕ_{DP} value.

Figures 5a,b show scatterplots of (a) $A_H(X)$ versus $K_{DP}(X)$, and (b) $A_{DP}(X)$ versus $K_{DP}(X)$. Because of the nearly linear relationship (see Table 1) in Figs. 5a,b it may be feasible to correct $Z_H(X)$ and $Z_{DR}(X)$ using K_{DP} measurements. Again assuming that Z_H and Z_{DR}
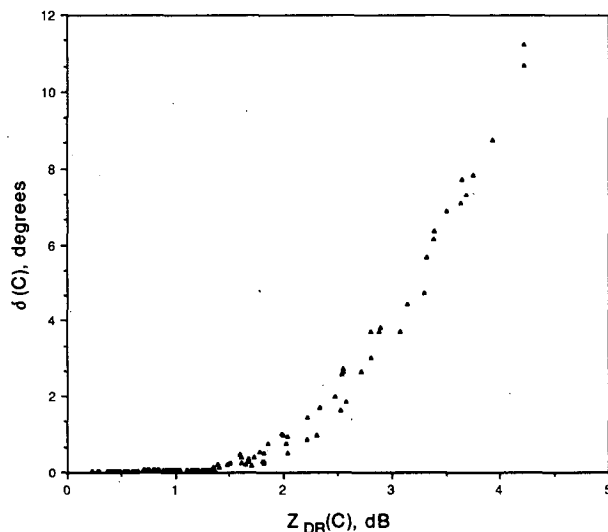

FIG. 5. (a) As in Fig. 1a except simulations are at X-band. (b) As in Fig. 1c except simulations are at X-band.

FIG. 4. Simulations of backscatter differential phase between H and V-polarizations, δ, versus differential reflectivity. Calculations are at C-band.
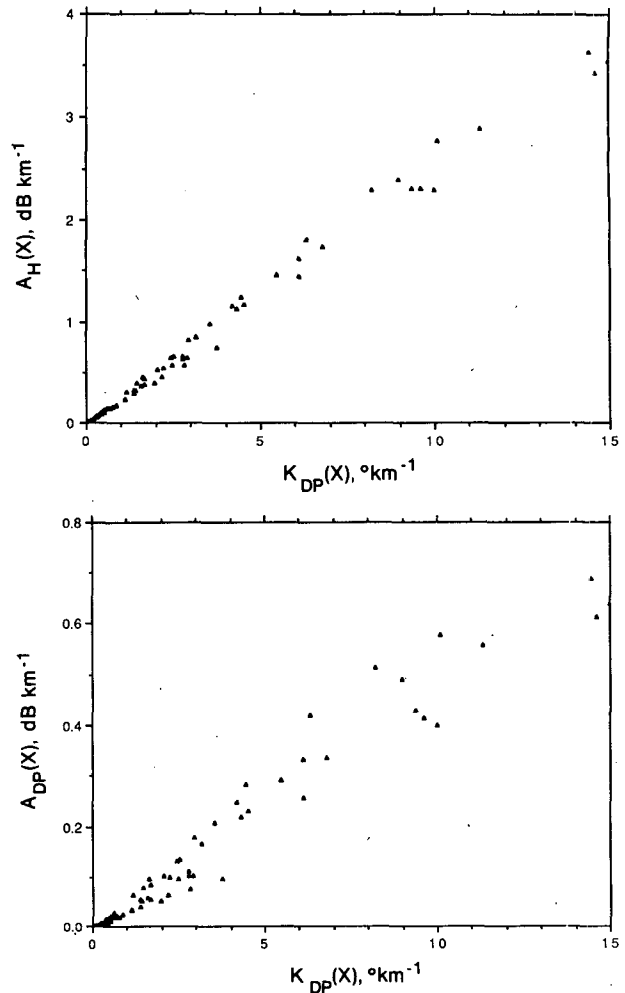
biases must be below 1.0 and 0.2 dB, respectively, correction is needed if $\phi_{DP}(X) \gtrsim 5°$. The previous remarks about the accuracy of the correction procedure due to the $\delta(X)$ apply here also.

3. Simulations based on disdrometer measurements

In the previous section, the variability of gamma parameters was chosen to reflect a wide variety of rainfall types; Ulbrich (1983). It is useful to see if the results of section 2 are consistent with simulations based on disdrometer measurements of RSDs at a single location.

An impact type disdrometer, developed by Rowland (1976), has been used for measuring the drop-size distributions. This disdrometer has a diameter of two inches, and measures drop sizes in 57 size categories, from 0.2 mm to 5.8 mm, with a resolution of 0.1 mm. Each distribution is obtained after the disdrometer has sampled 2000 drops. Hence, the sampling time and
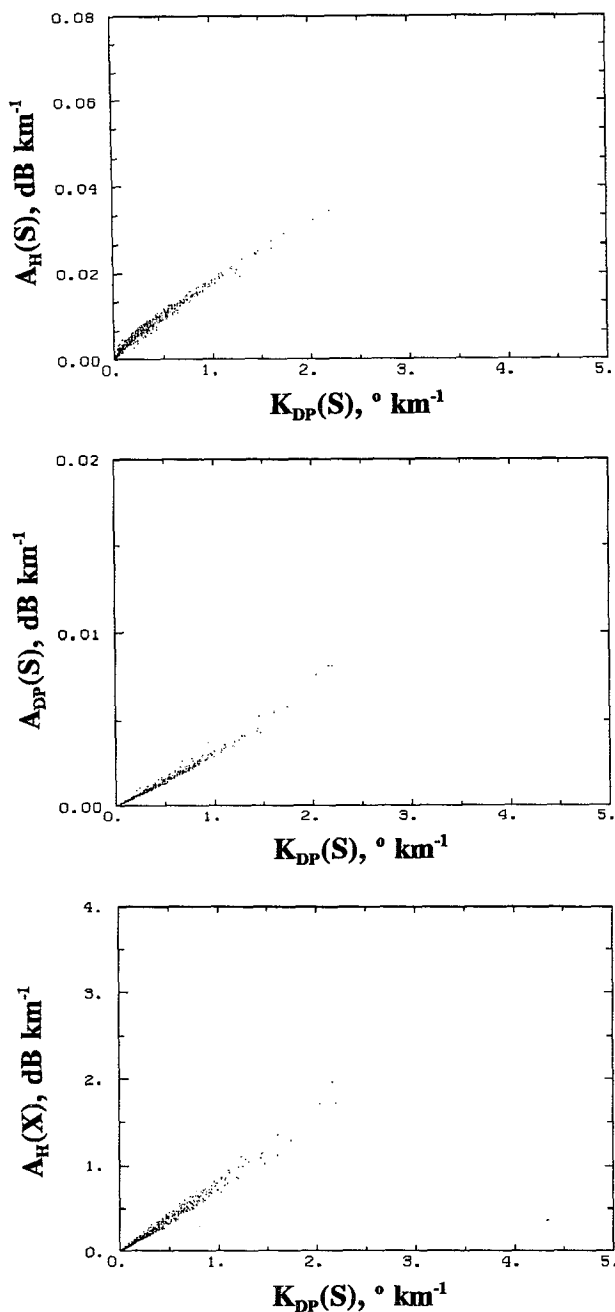
is the terminal velocity in m s^{-1}, and t is the sampling time in seconds. The drop diameter to terminal velocity relationship is taken as $v(D) = 3.778(D)^{0.67}$ m s^{-1} where D is in mm; Atlas and Ulbrich (1977).

The database examined consisted of 696 distributions obtained at the National Severe Storms Laboratory in Norman, Oklahoma, during three rain days; namely, (i) 14 May 1986, (ii) 16 May 1986, and (iii) 4 June 1986; see Balakrishnan et al. (1989) for details. A tipping bucket rain gauge, located nearby, was also used to measure the rainrate, and it was found to agree well with the rainrate derived from the disdrometer data.

In the simulation of radar measurands, the axis ratio of rain drops is obtained from Green (1975). The refractive index of water at 15°C is taken from Ray (1972) for S-band (3.0 GHz), C-band (5.5 GHz), and X-band (10.0 GHz).

Figures 6a, 7a, 8a show scatterplots of A_H versus K_{DP} at S-, C-, and X-bands, respectively. The S- and C-band simulations show less scatter than at X-band, although all three relationships are linear as seen from Table 2. These data are in good agreement with similar calculations based on the gamma RSD; e.g., compare Figs. 1a, 3a, 5a with Figs. 6a, 7a, 8a, respectively, and

FIG. 6. (a) Simulations of specific attenuation at H-polarization versus specific differential phase. Each data point is computed from an experimentally measured raindrop size distribution. Calculations are at S-band. (b) As in Fig. 6a except the ordinate scale is the specific differential attenuation between H and V polarizations, $A_{DP} = A_H - A_V$. (c) As in Fig. 6a except the ordinate scale is X-band specific attenuation at H-polarization. Note $A_H = 0.793K_{DP}$, rms deviation is 0.0307, and correlation coefficient is 0.994.

the sampling volume are dependent on the rainrate. It is typically 25 s when the rainrate is 20 mm h^{-1}. The sampling volume is equal to $\eta v(D)t$ where η is the sampling area of the disdrometer in m^2, and $v(D)$
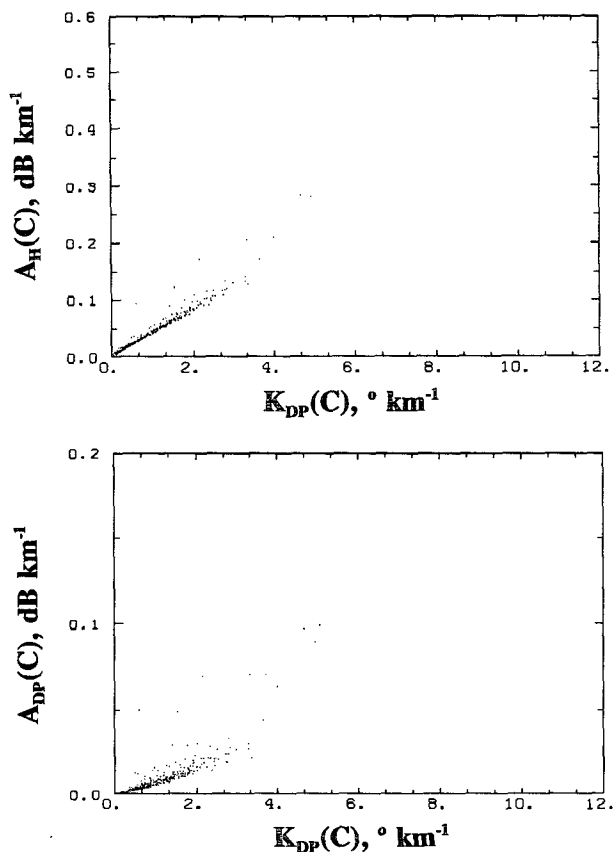
FIG. 7. (a) As in Fig. 6a except calculations are at C-band. (b) As in Fig. 6b except calculations are at C-band.
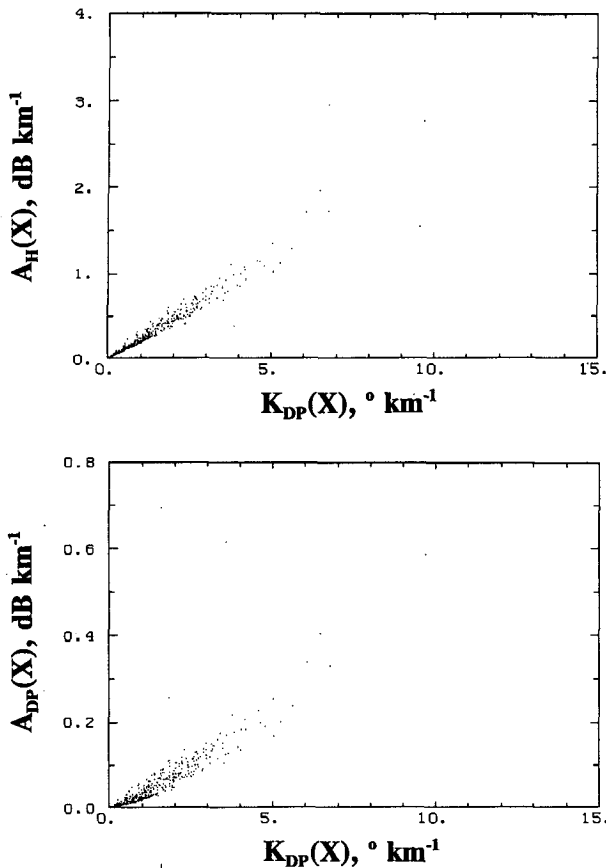
FIG. 8. (a) As in Fig. 6a except calculations are at X-band. (b) As in Fig. 6b except calculations are at X-band.

also Tables 1 and 2. The smaller spread seen in Figs. 6a, 7a, and 8a indicates that the variability of natural rain on the three days was less than the simulated variability. Figures 6b, 7b, 8b show scatterplots of A_{DP} versus K_{DP} at S-, C-, and X-bands, respectively. These can be compared to the gamma RSD calculations shown in Figs. 1c, 3b, 5b, which again show good agreement in that with decreasing frequency the scatter decreases. Figure 6c describes $K_{DP}(S)$ versus $A_H(X)$, which is similar to Fig. 1b. The gamma RSD parameter variations deduced by Ulbrich (1983) cover an unusually wide range of rainfall types whereas the disdrometer measurements were acquired at one location and three

days of one season. Thus, the gamma simulations show more variability than the disdrometer simulations. The mean relationships, however, are in good agreement as seen from Tables 1 and 2.

4. Radar measurements

During the Convection Initiation and Downburst Experiment (CINDE, Wilson et al. 1988) the NCAR CP-2 radar was used to gather time series data in convective rainshafts from which $A_H(X)$ and $K_{DP}(S)$ were estimated. Figures 9a,b show range profiles of the DFR; i.e., 10 $\log Z_H(S)$–10 $\log Z_H(X)$, (Eccles and Mueller 1973), and $\phi_{DP}(S)$ computed using the Mueller (1984) algorithm. These data were obtained in 1987 at low elevation angle through a convective rainshaft. The average rainrate in the range interval 86–93 km is 85 mm hr^{-1}. The data shown here have not been smoothed. Note the similar behavior of DFR and $\phi_{DP}(S)$ with increasing range and even a good correspondence between individual peaks in a region of significant rainfall (beyond 86 km).

Radar measurements obtained from convective rain events on three different days during CINDE were analyzed. Time series data were gathered at low elevation angles through the core of convective rainshafts over a time period of a few minutes. The processing technique used to reduce the statistical fluctuations in both DFR and $\phi_{DP}(S)$ is described in the Appendix. $A_H(X)$ and $K_{DP}(S)$ were obtained using this technique. The reflectivity field (Z_H) was filtered in range using a weighted, moving average filter. Figure 10a shows the results where $A_H(X)$ has been averaged over 0.2° km^{-1} categories of $K_{DP}(S)$. The vertical bars correspond to the standard deviation. The solid line is a least squares fit to the simulation data of Fig. 1b. The radar data are in excellent agreement with the gamma RSD model. Figure 10b shows the corresponding plot of $Z_H(S)$ versus $K_{DP}(S)$ where the averaging is done over 0.2° km^{-1} categories of $K_{DP}(S)$. The solid line is a power law fit to gamma RSD simulations of the relation between $Z_H(S)$ and $K_{DP}(S)$. These radar data show that attenuation prediction at higher microwave frequencies based on S-band differential propagation phase is feasible. Similar conclusions also apply to the prediction of differential attenuation.

TABLE 2. Mean linear relationships obtained using disdrometer measurements of raindrop size distributions. β is in dB per degree and ρ is the correlation coefficient.

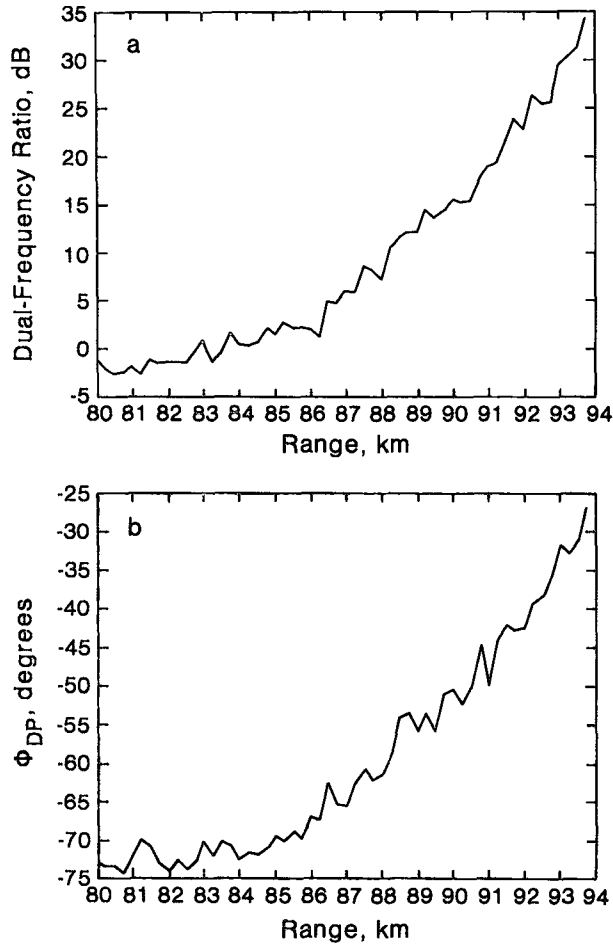|	Frequency band								
	S (3.0 GHz)			C (5.5 GHz)			X (10.0 GHz)		
Relation	β	ρ	rms dev.	β	ρ	rms dev.	β	ρ	rms dev.
$A_H = \beta K_{DP}$	0.0165	0.986	9.66×10^{-4}	0.05	0.965	1.07×10^{-2}	0.247	0.987	4.45×10^{-2}
$A_{DP} = \beta K_{DP}$	0.00334	0.989	1.73×10^{-4}	0.0139	0.83	7.3×10^{-3}	0.0458	0.961	1.45×10^{-2}

FIG. 9. CP-2 radar measurements of (a) the dual-frequency reflectivity ratio in dB versus range, and (b) the two-way differential propagation phase between H and V-polarizations, ϕ_{DP}, versus range. Data have not been smoothed. The dual-frequency reflectivity ratio in dB is the difference between the range normalized received powers at S- and X-bands. Data were obtained with antenna pointing in a convective rainshaft. The average rainrate in the interval 86–93 km is 85 mm h⁻¹.

5. Accuracy of correction procedures at S- and C-bands

The accuracy of correction procedures will depend mainly on three factors, (i) RSD fluctuations, (ii) variability in the estimate of $\arg(\hat{\rho}_{HV})$ due to measurement fluctuations, and (iii) to nonzero values of δ. Factors (i) and (ii) were simulated assuming $\delta = 0$ at S- and C-bands based on the model description that follows.

The $\arg(\hat{\rho}_{HV})$ measurement involves "pulse-pair" type algorithms for estimation of differential phase shifts, Mueller (1984), Sachidananda, and Zrnić (1986). Fluctuations in these estimates can be related to the width (σ_v) of the Doppler spectrum. Zrnić (1975) has developed a procedure for simulating univariate signal samples assuming a Gaussian form for the Doppler spectrum. Chandrasekar et al. (1986) generalized this procedure to simulate a bivariate time series

from which Z_{DR} could be estimated. The same bivariate signals can also be used to estimate $\arg(\hat{\rho}_{HV})$ using Mueller's (1984) algorithm. Signals corresponding to the two polarizations and having the same Doppler spectrum are independently simulated at two ranges, say, r_1 and r_2. The propagation path is defined to be the range interval (r_2-r_1) which is characterized by a constant K_{DP}. The simulated mean $\phi_{DP}(r_2)$ is obtained from mean $\phi_{DP}(r_1)$ by adding $2K_{DP}(r_2-r_1)$.

The principal assumptions and conditions are as follows:

- Gaussian Doppler spectrum with σ_v varying between 1 and 6 m s⁻¹. The quantity σ_v is linearly proportional to reflectivity in the range 0 to 55 dBZ.
- 128 samples at each polarization.
- Pulse repetition time of 1 m s.
- Radar wavelength of 10.0 or 5.5 cm.
- Zero-lag cross correlation ($|\rho_{HV}|$) of 0.99.
- $r_2-r_1 = 5$ km.
- Physical fluctuations in the gamma parameters (N_0, D_0, n) over the range specified in section 2.
- K_{DP} is constant over the 5 km one-way path. There is no loss of generality in this assumption because the relationships between α_H, α_{DP} and ϕ_{DP} are linear.

The following variables are defined:

$\phi_{DP}^{sm}(r)$—estimate of ϕ_{DP} from radar simulations at range r. The superscript "sm" stands for simulations.

$\Delta\phi_{DP}^{sm}$—$\phi_{DP}^{sm}(r_2) - \phi_{DP}^{sm}(r_1)$.

α_H^{sm}—estimate of α_H based on $\Delta\phi_{DP}^{sm}$ and the mean in Fig. 1a or Fig. 3a depending on frequency.

α_{DP}^{sm}—estimate of α_{DP} based on $\Delta\phi_{DP}^{sm}$ and the mean in Fig. 3b.

α_H^{sd}—estimate of α_H using the gamma RSD. The superscript "sd" stands for size distribution.

α_{DP}^{sd}—estimate of α_{DP} using the gamma RSD.

Figure 11 shows the simulation results at S-band as a scatterplot of α_H^{sm} versus α_H^{sd}. From the simulated ϕ_{DP} at r_1 and r_2, $\Delta\phi_{DP}^{sm}$ is obtained and converted to α_H^{sm} using the mean values in Fig. 1a. This process is repeated for different gamma RSDs. Thus the fluctuations in Fig. 11 include measurement error as well as gamma RSD variations. The fact that α_H^{sm} closely follows α_H^{sd} with very little scatter indicates the feasibility of accurate attenuation correction at S-band. The correction accuracy is ~0.05 dB independent of the mean value. If reflectivity estimates biased to less than 1 dB are desired, then the correction procedure can be implemented if $\phi_{DP}(S) \geq 60°$, see also, section 2.

Figure 12a shows similar simulation results at C-band. Note the increased scatter relative to Fig. 11. The correction accuracy is estimated to be within ~30% of the mean at C-band. If the measured $\phi_{DP}(C)$ $\leq 60°$ then the corrected reflectivity will be accurate to within 1 dB assuming that special processing tech-
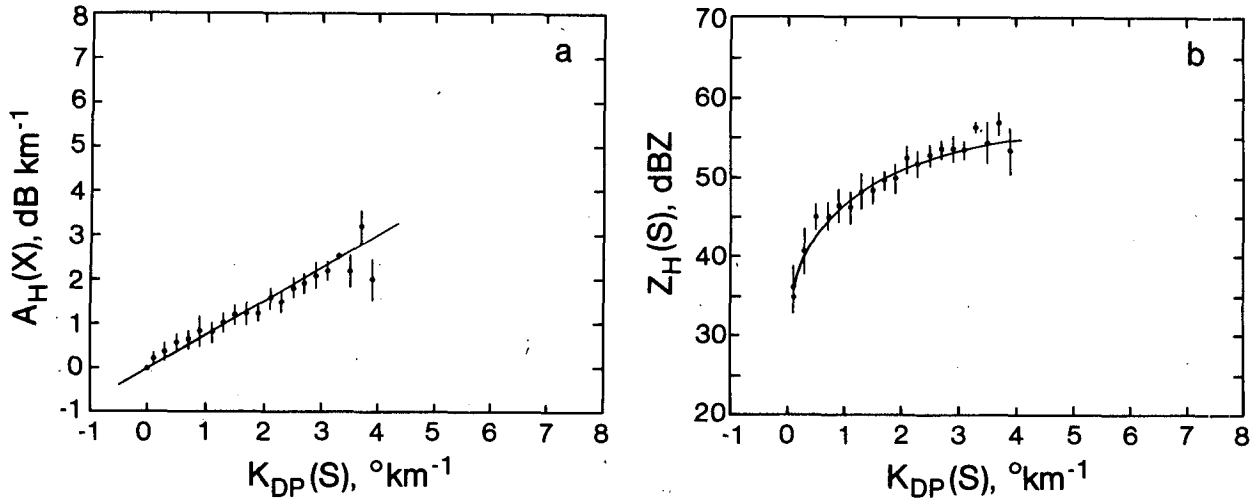
FIG. 10. CP-2 radar measurements of, (a) X-band specific attenuation, and (b) S-band reflectivity, versus the specific differential phase, K_{DP}. Data have been averaged over 0.2° km^{-1} categories of K_{DP}. Vertical bars represent the standard deviation. Radar data from several rainshafts on three different days have been combined. The solid line refers to a mean relationship obtained from gamma RSD simulations.

niques can account for δ. Figure 12b shows C-band simulation results of α_{DP}^{sm} versus α_{DP}^{sd}. The correction accuracy for differential attenuation is estimated to be within ~35% of the mean. This implies that $Z_{DR}(C)$ can be corrected to within, say, 0.3 dB if $\phi_{DP}(C) \lesssim 60°$. However, in an operational situation it would be desirable to correct for attenuation even if ϕ_{DP} exceeds 60°.

6. Conclusions

In this paper propagation effects such as attenuation, differential attenuation, and differential propagation
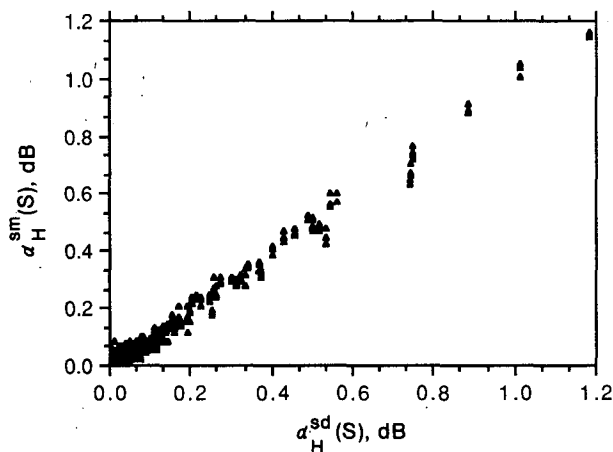

FIG. 11. Simulations at S-band of two-way attenuation at H-polarization versus the "exact" attenuation. Each data point refers to one triplet of gamma parameters (N_0, D_0, n) onto which random measurement errors have been superimposed. This figure shows how accurately S-band reflectivity estimates can be corrected for attenuation by rain using the measured ϕ_{DP}.

phase in rainfall are examined at microwave frequencies corresponding to S (3.0 GHz), C (5.5 GHz), and X (10.0 GHz) bands. Calculations using gamma RSDs, and simulations using disdrometer measured RSDs at one location are used to show that both attenuation and differential attenuation can be linearly related to differential propagation phase. A method to correct radar-measured reflectivity and Z_{DR} at attenuating frequencies is proposed if the differential propagation phase can be measured by the same radar. Measurements of X-band specific attenuation and S-band specific differential phase in convective rainshafts using the NCAR/CP-2 radar are presented in order to experimentally demonstrate the linear relationship between attenuation and differential propagation phase. Random measurement errors as well as natural fluctuations in the RSD were simulated to investigate the accuracy of the correction procedures at S- and C-bands. Backscatter differential phase (δ) effects are not considered in the simulations. The correction accuracy for S-band attenuation was estimated to be ~0.05 dB. If S-band reflectivity estimates accurate to within 1 dB are desired, corrections need not be made for ϕ_{DP} $\lesssim 60°$. If $\phi_{DP} > 60°$, then reflectivity estimates have bias greater than 1 dB and require correction procedures. At C-band and higher frequencies, nonzero values of the backscatter differential phase shift (δ) in rain and melting ice will further complicate the correction procedure. C-band simulations with $\delta = 0$ indicate that reflectivity estimates biased by less than 1 dB can be obtained if $\phi_{DP}(C) \lesssim 20°$. For $20° \lesssim \phi_{DP} \lesssim 60°$ the accuracy with which bias in reflectivity estimates can be corrected is within 1 dB. For larger ϕ_{DP} this accuracy will deteriorate further but is still recommended for operational purposes. Correction accuracy for attenuation at C-band is estimated to be within ~30% of
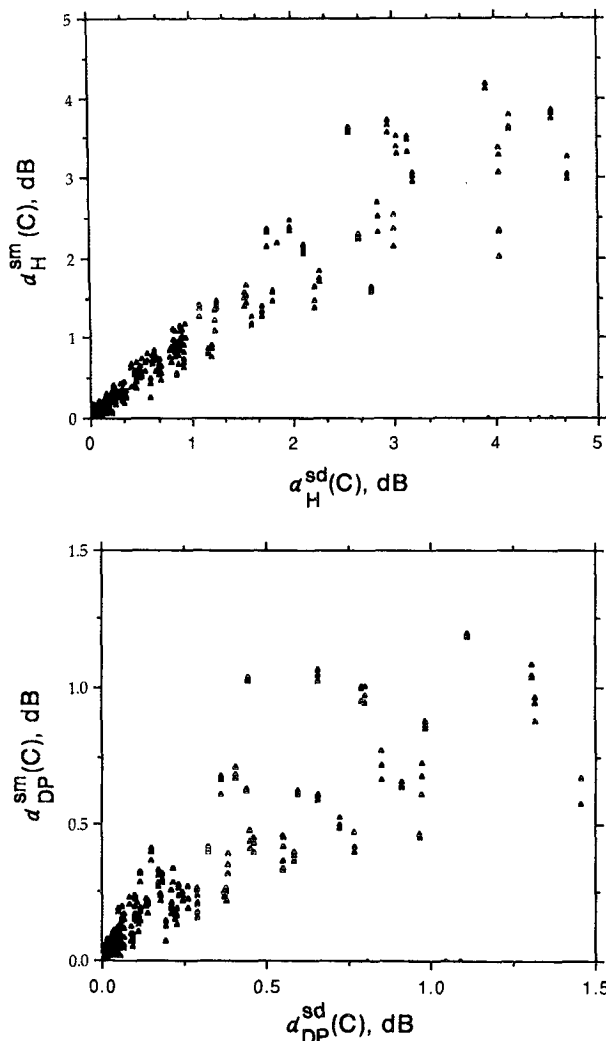
FIG. 12. (a) As in Fig. 11 except simulations are at C-band. (b) As in Fig. 11 except ordinate and abscissa scales refer to the C-band two-way differential attenuation. This figure shows how accurately C-band differential reflectivity estimates can be corrected for differential attenuation due to rain using the measured ϕ_{DP}.

the mean. Simulations indicate that C-band differential attenuation can be corrected to within ~35% of the mean value. This implies that Z_{DR} can be corrected to within, say, 0.3 dB if $\phi_{DP}(C) \leqslant 60°$.

the assistance rendered by Dr. Y. Golestani of CSU in processing the CP-2 radar data.

APPENDIX

Processing Technique for Reducing Statistical Fluctuations in DFR and ϕ_{DP}

In rainfall the DFR is a nondecreasing function of range; Eccles and Mueller (1973). At any range r we can write,

$$DFR(r) = \overline{DFR}(r) + \epsilon(r) \qquad (A1)$$

where $\overline{DFR}(r)$ is the mean value and $\epsilon(r)$ the fluctuating component. Consider two ranges r_1 and r_2 with $r_2 > r_1$, then

$$\overline{DFR}(r_2) - \overline{DFR}(r_1) = 2 \sum_{r_1}^{r_2} A(r)dr \qquad (A2)$$

where $A = A_H(X)$. Using finite differences, A can be expressed as

$$\overline{DFR}(r + \Delta r) - \overline{DFR}(r) = 2A(r)\Delta r. \qquad (A3)$$

The dual-frequency radar measures $DFR(r_i)$ where $i = 1, 2, \cdots n$, the range increment corresponding to the range gate spacing that is 150 m for the CP-2 radar. To extract $\overline{DFR}(r_i)$ from $DFR(r_i)$, the fluctuations $\epsilon(r_i)$ need to be modeled. Since signals from different range gates are statistically independent, $\epsilon(r_j)$ and $\epsilon(r_i)$ are independent if $j \neq i$. We also need to know the relative variances of $\epsilon(r_i)$ to weight the fluctuations. However, if the processing is done using the dB scale for DFR we have uniform variance of $\epsilon(r_i)$ along the range and the problem is simplified. Thus, we fit a nondecreasing polynomial to $DFR(r)$ that is valid in rainfall according to the model:

$$DFR(r) = \beta_0 + \beta_1 r + \beta_2 r^2 + \cdots + \epsilon(r). \qquad (A4)$$

The coefficients β_i are evaluated by minimizing the variance of $\epsilon(r)$ for all r. The polynomial on the right-hand side of Eq. (A3) equals $\overline{DFR}(r)$. The specific attenuation A can be calculated as

$$A = (\beta_1 + 2\beta_2 r + \cdots)/2. \qquad (A5)$$

The order of the polynomial needs to be chosen to fit the DFR (r) data. The optimum function would cause the variance of $[DFR(r) - \overline{DFR}(r)]$ to equal the measurement variance of $DFR(r)$. Based on an analysis of variance for a number of paths in convective rainfall, we have determined that a third-order polynomial approximately satisfies the above criterion. This procedure was also applied to the ϕ_{DP} data.

REFERENCES

Atlas, D., and C. W. Ulbrich, 1977: Path and area-integrated rainfall measurements by microwave attenuation in the 1-3 cm band. *J. Appl. Meteor.,* **16,** 1622-1631.

——, —— and R. Meneghini, 1984: The multiparameter remote measurement of rainfall, *Rad. Sci.*, **19**, 3–20.

Aydin, K., Y. Zhao and T. A.. Seliga, 1989: Rain-Induced Attenuation Effects on C-band Dual-Polarization Meteorological Radars. *IEEE Trans. Geosci. Remote Sens.*, **27**, 57–66.

Balakrishnan, N., D. S. Zrnić, J. Goldhirsh and J. Rowland, 1989: Comparison of simulated rain rates from disdrometer data employing polarimetric radar algorithms. *J. Atmos. Oceanic. Technol.*, **6**, 476–486.

Bebbington, D. H. O., R. McGuiness and A. R. Holt, 1987: Correction of propagation effects in S-band circular polarization-diversity radars. *Proc. IEE*, **34**, 431–437.

Bringi, V. N., V. K. Varadan and V. V. Varadan, 1983: Average dielectric properties of discrete random media using multiple scattering theory. *IEEE Trans. Antennas and Propag.*, **31**, 371–375.

Chandrasekar, V., V. N. Bringi and P. J. Brockwell, 1986: Statistical properties of dual-polarized signals. *23rd AMS Conf. Radar Meteorology*, Amer. Meteor. Soc., 193–196.

Doviak, R. J., and D. S. Zrnić, 1984: *Doppler Radar and Weather Observations*, Academic Press,

Eccles, P. J., 1979: Comparison of remote measurements by single and dual-wavelength meteorological radars. *IEEE Trans. Geosci. Electron.*, 205–218.

——, and E. A. Mueller, 1973: X-band attenuation and liquid water content estimation by a dual-wavelength radar. *J. Appl. Meteor.*, **10**, 1252–1259.

Goddard, J. W. F., and S. M. Cherry, 1984: The ability of dual-polarization radar (copolar linear) to predict rainfall rate and microwave attenuation. *Rad. Science*, **19**, 201–208.

Green, A. W., 1975: An approximation for the shape of large raindrops. *J. Appl. Meteor.*, **14**, 1578–83.

Hendry, A., and Y. M. M. Antar, 1984: Precipitation particle identification with centimeter wavelength dual-polarization radar. *Rad. Science*, **19**, 115–122.

——, G. C. McCormick and B. L. Barge, 1976: KU-band and S-band observations of the differential propagation constant in snow. *IEEE Trans.* **24**, 521–525.

Hildebrand, P. H., 1978: Iterative correction for attenuation of 5 cm radar measurement of rainfall at attenuating wavelengths. *J. Meteor.*, **17**, 508–514.

Hitschfeld, W., and J. Bordan, 1954: Errors inherent in the radar measurement of rainfall at attenuating wavelengths. *J. Meteor.*, **11**, 58–67.

Holt, A. R., 1988: Extraction of differential propagation phase from data from S-band circularly polarized radars. *Electron. Lett.*, **24**, 1241–1242.

Holt, A. R., R. McGuiness and B. G. Evans, 1984: Frequency scaling propagation parameters using dual-polarization radar results. *Rad. Sci.*, **19**, 222–230.

Humphries, R. G., 1974: Depolarization effects at 3 GHz due to precipitation. Sci. Rep. MW–82, Stormy Weather Group, McGill University, Montreal, Canada.

Ishimaru, A., 1977: Theory and application of wave propagation and scattering in random media. *IEEE Proc.*, **65**, 1030–1061.

Jameson, A. R., 1985: Microphysical interpretation of multiparameter radar measurements in rain. Part III: Interpretation and measurement of propagation differential phase shift between orthogonal linear polarizations. *J. Atmos. Sci.*, **42**, 607–614.

——, 1989: Theoretical analysis and meteorological interpretation of the role of raindrop shape on microwave attuation and propagation phase shift: implications for the radar measurement of rain. *J. Atmos. Oceanic Technol.*, **6**, 76–88.

——, and R. C. Srivastava, 1978: Dual-wavelength Doppler radar observations of hail at vertical incidence. *J. Appl. Meteor.*, **17**, 1694–1703.

——, and E. A. Mueller, 1985: Estimation of propagation differential phase shift from sequential orthogonal linear polarization radar measurements. *J. Atmos. Oceanic. Technol.*, **2**, 133–137.

——, and J. H. Dave, 1988: An interpretation of circular polarization measurements affected by propagation differential phase shift. *J. Atmos. Oceanic. Technol.*, **5**, 405–415.

Leitao, M. J., and P. A. Watson, 1984: Application of dual linearly polarized radar data to prediction of microwave path attenuation at 10–30 GHz. *Rad. Science*, **19**, 209–221.

McCormick, G. C., and A. Hendry, 1975: Principles for the radar determination of the polarization properties of precipitation. *Radio Science*, **10**, 421–434.

Marshall, R. E., T. Pratt, E. A. Manus, D. P. Stapor and J. H. Andrews, 1984: S-band radar differential reflectivity measurements in multiple polarization planes along satellite slant paths. *Rad. Sci.*, **19**, 109–114.

McGuiness, R., D. H. O. Bebbington and A. R. Holt, 1987: Modeling propagation effects in the use of S-band polarization-diversity radars. *IEE Proc.*, **134**, 423–430.

Meischner, P. F., T. Jank, V. N. Bringi and J. Vivekanandan, 1989: Multiple plane Z_{DR} measurements in convective and stratiform clouds using the C-band polarimetric DFVLR radar. Preprints, *24th AMS Radar Meteorology Conf.*, Tallahassee, Florida, Amer. Meteor. Soc.

Mueller, E. A., 1984: Calculation procedure for differential propagation phase shift. Preprints, *22nd AMS Conf. on Radar Meteorology.* Zurich, Amer. Meteor. Soc., 397–399.

Oguchi, T., 1983: Electromagnetic wave propagation and scattering in rain and other hydrometeors. *IEEE Proc.*, **71**, 1029–1078.

Ray, P. S., 1972: Broad-band complex refractive indices of ice and water. *Appl. Opt.*, **11**, 1836–1844.

Rowland, J. R., 1976: Comparison of two different disdrometers. *17th AMS Conf. Radar Meteorology*, Seattle, Amer. Meteor. Soc.

Sachidananda, M., and D. S. Zrnić, 1987: Rain rate estimated from differential polarization measurements, *J. Atmos. Oceanic Technol.*, **4**, 588–598.

——, and ——, 1989: Differential Propagation Phase Shift and Rainfall Rate Estimation. *Rad. Sci.*, **21**, 235–247.

——, and ——, 1989: Efficient processing of alternately polarized radar signals. *J. Atmos. Oceanic. Technol.*, **6**, 173–181.

Seliga, T. A., and V. N. Bringi, 1976: Potential use of radar differential reflectivity measurements at orthogonal polarizations for measuring precipitation. *J. Appl. Meteor.*, **15**, 69–76.

——, and ——, 1978: Differential reflectivity and differential phase shift: applications in Radar Meteorology. *Rad. Sci.*, **13**, 271–275.

Twersky, V., 1978: Coherent electromagnetic waves in pair-correlated random distribution of aligned scatterers. *J. Math. Phys.*, **19**, 215–230.

Tuttle, J. D., and R. E. Rinehart, 1983: Attenuation correction in dual-wavelength analyses. *J. Climate Appl. Meteor.*, **22**, 1914–1921.

Ulbrich, C. W., 1983: Natural variations in the analytical form of raindrop size distribution. *J. Climate Appl. Meteor.*, **22**, 1764–1775.

Wilson, J. W., J. A. Moore, G. Brant Foote, B. Martner, A. R. Rodi, T. Uttal and J. M. Wilczak, 1988: Convection Initiation and Downburst Experiment (CINDE), *Bull. Amer. Meteor. Soc.*, **69**, 1328–1348.

Zrnić, D. S., 1975: Simulation of weatherlike Doppler spectra and signals. *J. Appl. Meteor.*, **14**, 619–620.